Contribution from the Laboratoire de chimie appliqueé de l'état solide (URA 1466 CNRS) and Laboratoire de chimie organometallique (URA 403 CNRS), Ecole Nationale Superieure de Chimie de Paris, 11 rue P. et M. Curie, 75005 Paris, France, and Afdeling Anorganische Chemie, Universiteit Nijmegen, 63 Toernooiveld, NL-6525 ED Nijmegen, The Netherlands

Bis(cyclooctatetraene)vanadium: X-ray Structure and Study of Molecular Motions by EPR and ENDOR Spectroscopy in Frozen Solution

Didier Gourier,*,† Edmond Samuel,*,‡ Bernd Bachmann, Friedemann Hahn, and Jürgen Heck*,§

Received December 28, 1990

The paramagnetic $V(cot)_2$ (cot = η^8-C_8H_8) was obtained in high yields from $VCl_3(THF)_3$ and a mixture of cyclooctatetraene with its potassium salt. The X-ray structure shows that the metal is bound to one ring in an η^8 and to the other ring in a η^4 fashion, with two different molecules in the unit cell. The complex crystallizes in the orthorhombic space group $P2_12_12_1$ with a = 825.9 (1) pm, b = 1145.6 (2) pm, c = 2560.4 (4) pm, V = 2422.5 Å^3, and Z = 8. Refinement of 5392 reflections yielded R = 0.0388 and R_w = 0.0364. In frozen solution, EPR parameters show that the unpaired electron resides in a nonbonding orbital having mainly a d_{z^2} character. Proton hyperfine interactions were determined by ENDOR for the different types of (η^8-C_8H_8) and (η^4-C_8H_8) ring protons, in agreement with the bonding scheme revealed by the crystal structure. Variable-temperature ENDOR studies from 9 to 150 K gave information about molecular motion such as ring fluxionality and molecular tumbling in the solid state. It is also shown that upon slow cooling partial alignment of the complex along the magnetic field axis occurs.

Introduction

Sandwich complexes of the formula $M(C_nH_n)_2$ (M = transition metal; n = 4-8) containing 14-20 valence electrons are well-known[1] and their crystal as well as electronic structures[2] are established in most cases, especially for the first-row transition metals. One exception in this series is the paramagnetic complex $V(cot)_2$ (**1**), the synthesis of which was briefly described[3] in 1966, but whose geometry and electronic structure remained a subject of some controversy.[4,5] In our quest for mononuclear cot complexes as precursors for heterobinuclear compounds with bridging cot units,[6] we describe in this work a new and simple synthesis giving **1** in high yields. We also present the crystal structure results showing that the metal is bound to one ring in an η^8 and to the other in an η^4 fashion, supported by detailed EPR and ENDOR studies, thus providing sufficient evidence for a reliable knowledge of this molecule.

Six years after the discovery of **1**,[3] Thomas and Hayes[4] reported its EPR parameters. More recently Hocks et al.[5] described an EPR spectrum with completely different parameters, and concluded that the unpaired electron resides in a molecular orbital with metallic d_{yz} character, which is in disagreement with Thomas and Hayes' results showing that the SOMO is d_{z^2} as expected for this family of compounds. In order to explain their findings, Hocks et al. performed a molecular orbital calculation on the basis of a V(η^8-C_8H_8) half-sandwich entity weakly bonded to the other (C_8H_8) ring. It will be shown in this work that this model is in complete disagreement with the crystal structure, which shows that both rings are strongly bonded to the metal atom. It thus appeared interesting to reinvestigate the EPR of **1** in order to explain the discrepancy between the two early EPR studies.[3,4]

A consequence of the peculiar structure of **1** is its aptitude to nonrigidity, and the first kind of intramolecular motion imaginable is a fast rotation of the (η^8-C_8H_8) ring around the vanadium-ring direction, as with other parent sandwich (η^8-C_8H_8) derivatives.[7,8] A second kind is a metal shift within the η^4-bonded C_8H_8 ring. It was shown by NMR[9] that all the known diamagnetic (η^4-C_8H_8) derivatives are more or less fluxional. To our knowledge, this kind of intramolecular motion has hitherto not been observed by EPR on a paramagnetic (1,4-η^4-C_8H_8) compound. Moreover, in diamagnetic (1-4,η^4-C_8H_8)M(η^8-C_8H_8) compounds (M = Ti, Ta, Nb)[9,10] NMR provides evidence for another kind of fluxionality which concerns a fast interchange of η^4- and η^8-bonded C_8H_8 rings. All these phenomena are therefore liable to exist in the title compound.

Table I. Principal Experimental Parameters of the X-ray Structure Analysis and Crystal Data for (η^8-cot)V(η^4-cot) (**1**)

chem formula	$C_{16}H_{16}V$	Z	8
fw	259.2	space group	$P2_12_12_1$
a, Å	8.259 (1)	ρ_{calcd} g/cm^3	1.422
b, Å	11.456 (2)	μ, cm^{-1}	7.33
c, Å	25.604 (4)	R	0.0388
cell vol, Å^3	2422.5	R_w	0.0364

The observation of these different types of rearrangements in **1** necessarily implies the detection of the vanadium-proton hyperfine (hf) interactions, which were not resolved in the previous EPR investigations.[4,5] In sandwich compounds, ENDOR spectroscopy when conducted on dilute single crystals,[11] powders,[12] or frozen solutions[7] allows one to measure these hf interactions accurately. It thus completes EPR spectroscopy, especially when ligand hf interactions are not resolved. Moreover, intramolecular motion, which results in a partial averaging of the metal-proton interaction,[11,12] presents dramatic effects in frozen-solution ENDOR spectra of pseudosandwich compounds.[7,8] The generally broad, powder-shaped ENDOR lines become narrow, often single crystal like. The coexistence of static and very mobile fragments in a complex becomes evident simply from the shape of the ENDOR lines.

Experimental Section

All manipulations were performed under nitrogen or argon with thoroughly dried solvents.

$V(cot)_2$ (1). To a cooled solution (-78 °C) of 5.6 g (15.0 mmol) of VCl_3·3THF in 120 mL of THF are added dropwise 60 mL of a THF solution containing 23 mmol of $K_2(C_8H_8)$ and 8 mmol of C_8H_8, and the reaction mixture is allowed to warm up to room temperature, while the color changes from green to dark brown. After additional 24 h of stirring, the solvent is stripped off in vacuum and the residue is extracted

† Laboratoire de chimie appliquée de l'état solide (URA 1466 CNRS), Ecole Nationale Superieure de Chimie de Paris.

‡ Laboratoire de chimie organométallique (URA 403 CNRS), Ecole Nationale Superieure de Chimie de Paris.

§ Universiteit Nijmegen.

(1) Elschenbroich, C.; Salzer, A. *Organometallics* **1989**, *8*, 309.
(2) (a) Mingos, D. M. P. In *Comprehensive Organometallic Chemistry*; Wilkinson, G., Stone, F. G. A., Abel, E. W., Eds.; Pergamon Press: Oxford, England, 1982; Vol. 3, p 1. (b) Clack, D. W.; Warren, K. D. *Struct. Bonding* **1980**, *39*, 1. (c) Muetterties, E. L.; Bleeke, J. R.; Wucherer, E. J.; Albright, T. A. *Chem. Rev.* **1982**, *82*, 499. (d) Weber, J.; Geoffroy, M.; Goursot, A.; Penigault, E. *J. Am. Chem. Soc.* **1978**, *100*, 3995.
(3) Breil, H.; Wilke, G. *Angew. Chem.* **1966**, *78*, 942; *Angew. Chem., Int. Ed. Engl.* **1966**, *5*, 898.
(4) Thomas, J. L.; Hayes, R. G. *Inorg. Chem.* **1972**, *11*, 348.
(5) Hocks, L.; Hubin, R.; Goffart, J. *J. Organomet. Chem.* **1976**, *104*, 199.
(6) (a) Bachmann, B.; Baum, G.; Heck, J.; Massa, W.; Ziegler, B. *Z. Naturforsch. B* **1990**, *45*, 221. (b) Bachmann, B.; Hahn, F.; Heck, J. *Organometallics* **1989**, *8*, 2523.
(7) Gourier, D.; Samuel, E. *J. Am. Chem. Soc.* **1987**, *109*, 4571.
(8) Gourier, D.; Samuel, E.; Teuben, J. *Inorg. Chem.* **1989**, *28*, 4662.
(9) Schrock, R. R.; Guggenberger, L. J.; English, A. D. *J. Am. Chem. Soc.* **1976**, *98*, 903.
(10) Schwartz, J.; Sadler, J. E. *J. Chem. Soc., Chem. Commun.* **1973**, 903.
(11) Wolf, R.; Schweiger, A.; Gunthard, H. H. *Mol. Phys.* **1984**, *53*, 585.
(12) Schweiger, A.; Wolf, R.; Gunthard, H. H.; Ammeter, J. H.; Deiss, E. *Chem. Phys. Lett.* **1980**, *71*, 117.

0020-1669/92/1331-0086$03.00/0

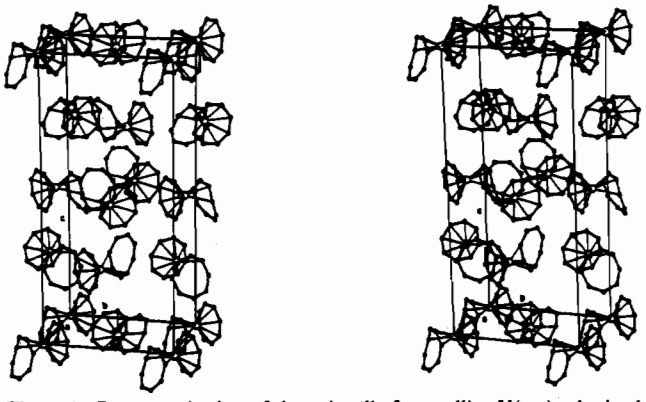

Figure 1. Stereoscopic view of the unit cell of crystalline $V(cot)_2$ obtained from the X-ray structure analysis.

with boiling toluene to separate KCl from the product. Yield (not optimized): 2.8 g (72% based on VCl_3). Mp: >230 °C. EI-MS *m/e* (%): 260 (7.6) $M^+ + 1$, 259 (44.3) M^+, 155 (100) $Vcot^+$, 129 (20.1) $VC_6H_6^+$, 116 (14.0) $C_5H_5^+$, 104 (9.3) $C_8H_8^+$, 103 (9.5) $C_8H_7^+$, 91 (6.6) $C_7H_7^+$, 51 (29.7) V^+. Anal. Calcd for $C_{16}H_{16}V$ (M = 259.54): C, 74.12; H, 6.22. Found: C, 74.24; H, 6.39.

X-ray Data Collection, Structure Determination, and Refinement. Suitable crystals of **1** were grown by a slow recrystallization from toluene at a small temperature gradient. A black single crystal was chosen with the approximate dimensions 0.78 × 0.72 × 0.42 mm³ and sealed under N_2 in a thin-walled quartz capillary.

Diffracted intensities were collected on an Enraf Nonius four-circle diffractometer (CAD4, ω scans) at −55 °C with graphite monochromator Mo Kα radiation. Final lattice parameters (Table I) are determined from least-squares refinement with $[(\sin\theta)/\lambda]^2$ values for 25 reflections ($12° < \theta < 21°$).

The crystal structure was solved by the direct methods[13] and refined with anisotropic thermal parameters.[14] All hydrogen atoms were located by difference Fourier synthesis and refined by isotropic thermal parameters. In the final cycles of the refinement the H atoms are fixed on "riding" positions. The reversal of the polarity within the noncentrosymmetric space group leads to considerably worse R values (R = 0.0442, R_w = 0.0416). A summary of the data collection parameters is given in Table I. The resulting atomic positional coordinates are listed in Table II.

Spectroscopic Measurements. Toluene or deuteriotoluene were used as solvents. For EPR and ENDOR, solutions were sealed under vacuum in quartz tubes. EPR spectra were recorded with a Bruker 220 D X-band spectrometer equipped with a standard TE_{102} cavity and a variable temperature accessory for temperatures in the range 100 $K < T <$ 300 K and with an Oxford Instruments ESR 9 continuous-flow helium cryostat for 4 K < T < 100 K. ENDOR experiments were performed in deuteriotoluene in order to avoid hf interactions with solvent protons. A Bruker cavity was used working in the TM_{110} mode with a 100-W ENI broadband power amplifier. Spectra were detected using frequency modulation of the rf carrier at a frequency of 12.5 kHz. With this modulation scheme, the ENDOR signal has the shape of the first derivative of the ENDOR enhancement.

Ligand abbreviations used: Cp = cyclopentadienyl (η^5-C_5H_5); (cot) = cyclooctatetraene (η^8-C_8H_8); (cht) = cycloheptatrienyl (η^7-C_7H_7); bu = butadiene; cbu = cyclobutadiene; bz = benzene (η^6-C_6H_6).

Synthesis and Structure Determination

The title compound **1** can be obtained in very good yields from the following reaction:

$$2VCl_3(THF)_3 + 3K_2(C_8H_8) + C_8H_8 \rightarrow 2V(cot)_2 + 6KCl$$

The advantages of this reaction compared to the previously known synthesis are the simple manipulation and easy storage of the adduct $VCl_3(THF)_3$ in contrast to VCl_4 and the high yield obtained. The reaction is conducted with excess cyclooctatetraene.

Table II. Final Fractional Coordinates (×10⁴) and Isotropic Thermal Parameters $U_{eq} = {}^1/_3(U_{11} + U_{22} + U_{33})$ (×10⁴ Å²) of (η^8-cot)V(η^4-cot) (**1**)

	x	y	z	U_{eq},[a] Å²
		Structure I		
V1	2419.5 (5)	8957.9 (3)	2476.3 (2)	290 (1)
C11	507 (4)	8718 (3)	1834 (1)	513 (10)
C12	−256 (4)	9210 (3)	2251 (2)	572 (13)
C13	−170 (4)	9110 (3)	2803 (2)	579 (12)
C14	822 (4)	8442 (3)	3150 (1)	527 (12)
C15	1978 (4)	7564 (2)	3078 (1)	447 (10)
C16	2605 (4)	6992 (2)	2644 (1)	424 (9)
C17	2470 (4)	7094 (2)	2112 (1)	428 (9)
C18	1663 (4)	7827 (3)	1770 (1)	458 (10)
C21	2745 (3)	10962 (2)	2578 (1)	423 (9)
C22	3875 (3)	10267 (2)	2854 (1)	362 (8)
C23	4918 (3)	9422 (2)	2657 (1)	418 (9)
C24	5282 (4)	9095 (3)	2142 (1)	456 (10)
C25	5363 (4)	9647 (3)	1654 (1)	497 (10)
C26	4755 (4)	10663 (3)	1443 (1)	479 (10)
C27	3556 (4)	11405 (3)	1619 (1)	530 (11)
C28	2638 (4)	11443 (3)	2068 (1)	538 (11)
H11	217 (3)	9054 (2)	1506 (1)	329 (68)
H12	−987 (3)	9748 (2)	2180 (1)	1061 (149)
H13	−754 (3)	9901 (2)	2981 (1)	490 (82)
H14	844 (3)	8653 (2)	3503 (1)	415 (81)
H15	2623 (3)	7434 (2)	3397 (1)	391 (73)
H16	3373 (3)	6613 (2)	2752 (1)	467 (90)
H17	3200 (3)	6824 (2)	1887 (1)	496 (92)
H18	2030 (3)	7715 (2)	1354 (1)	601 (91)
H21	1866 (3)	11125 (2)	2834 (1)	1387 (173)
H22	3829 (3)	10252 (2)	3246 (1)	318 (68)
H23	5356 (3)	9079 (2)	2895 (1)	559 (98)
H24	5764 (3)	8546 (2)	2114 (1)	465 (95)
H25	5883 (3)	9221 (2)	1377 (1)	869 (120)
H26	5054 (3)	10707 (2)	1055 (1)	622 (92)
H27	3184 (3)	11950 (2)	1303 (1)	952 (120)
H28	1646 (3)	11726 (2)	2025 (1)	1230 (166)
		Structure II		
V2	5425.0 (5)	4894.5 (3)	−13.2 (2)	260 (1)
C31	4992 (5)	3683 (4)	672 (2)	688 (2)
C32	5693 (5)	3021 (3)	297 (2)	765 (18)
C33	5619 (6)	2964 (3)	−242 (3)	848 (20)
C34	4774 (5)	3588 (4)	−632 (2)	728 (16)
C35	3572 (5)	4461 (4)	−612 (2)	708 (15)
C36	2726 (4)	5012 (3)	−218 (2)	664 (15)
C37	2831 (4)	5036 (3)	317 (2)	625 (14)
C38	3795 (5)	4502 (4)	679 (2)	712 (16)
C41	8275 (3)	5057 (2)	3 (1)	332 (7)
C42	7468 (3)	5736 (2)	−380 (1)	306 (7)
C43	6238 (3)	6579 (2)	−306 (1)	300 (8)
C44	5526 (3)	6981 (2)	164 (1)	328 (8)
C45	6061 (3)	7209 (2)	678 (1)	375 (9)
C46	7403 (3)	6922 (2)	966 (1)	390 (8)
C47	8591 (3)	6051 (2)	896 (1)	397 (9)
C48	8802 (3)	5228 (2)	516 (1)	381 (9)
H31	5415 (3)	3807 (2)	991 (1)	674 (106)
H32	6649 (3)	2428 (2)	421 (1)	1027 (136)
H33	6313 (3)	2657 (2)	−371 (1)	840 (149)
H34	5131 (3)	3549 (2)	−955 (1)	604 (98)
H35	3390 (3)	4716 (2)	−910 (1)	633 (105)
H36	2130 (3)	5424 (2)	−302 (1)	923 (154)
H37	2082 (3)	5793 (2)	468 (1)	527 (86)
H38	3767 (3)	4772 (2)	967 (1)	620 (112)
H41	8738 (3)	4488 (2)	−188 (1)	520 (93)
H42	7655 (3)	5489 (2)	−745 (1)	312 (65)
H43	5746 (3)	6837 (2)	−633 (1)	128 (57)
H44	4472 (3)	7375 (2)	77 (1)	295 (63)
H45	5238 (3)	7842 (2)	831 (1)	436 (74)
H46	7489 (3)	7234 (2)	1303 (1)	314 (66)
H47	9277 (3)	5954 (2)	1184 (1)	531 (85)
H48	9579 (3)	4704 (2)	620 (1)	686 (101)

[a] For H the isotropic temperature factors U_{iso} are taken.

The X-ray structure done on single crystals of **1** shows an orthorhombic crystal with an asymmetric unit consisting of two different molecules (named I and II). The unit cell is shown in

(13) Main, P.; Fiske, S. J.; Hull, S. E.; Lessinger, L.; Germain, G.; Declerq, J.-P.; Woolfson, M. M. Multan 80, A System of Computer Programs for Automatic Solution of Crystal Structures from X-Ray Diffraction Data. Universities of York (England) and Louvain (Belgium), 1980.
(14) Sheldrick, G. M. SHELX76. Program for Crystal Structure Determination. University of Cambridge, 1976; SHELX-86 (Program for Crystal Structure Solution). Universität Göttingen, 1986.

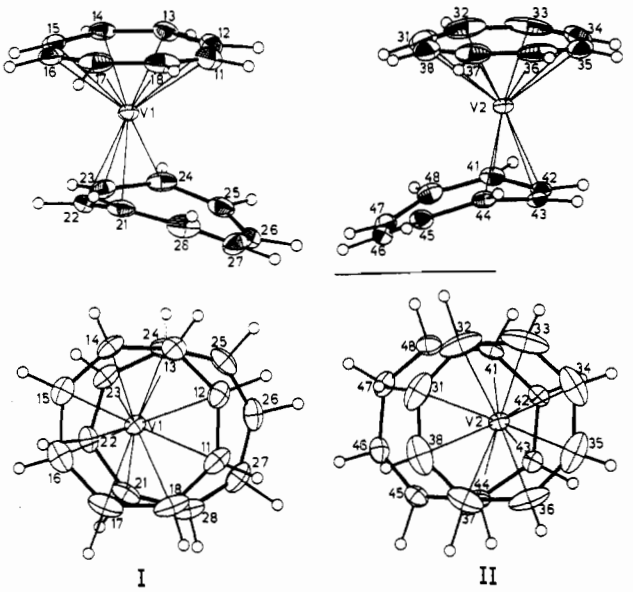

Figure 2. ORTEP view[16] of the molecular structure of $V(cot)_2$ with non-hydrogen atoms represented by their 30% probability ellipsoids for thermal motion: (above) side view; (below) projection perpendicular to the η^8-C_8 plane.

Table III. Selected Bond Distances (pm) of (η^8-cot)V(η^4-cot) (**1**)

V1–C11	229.7 (3)	V2–C31	226.4 (4)
V1–C12	231.7 (4)	V2–C32	229.8 (4)
V1–C13	230.3 (3)	V2–C33	229.4 (4)
V1–V14	224.9 (3)	V2–C34	224.5 (4)
V1–C15	224.9 (3)	V2–C35	222.2 (4)
V1–C16	229.8 (3)	V2–C36	229.4 (4)
V1–C17	233.0 (3)	V2–C37	230.9 (4)
V1–C18	231.2 (3)	V2–C38	227.1 (4)
V1–C_8[a]	139.2 (11)	V2–C_8[a]	138.8 (6)
V1–C21	232.7 (3)	V2–C41	236.1 (2)
V1–C22	215.2 (3)	V2–C42	216.0 (3)
V1–C23	218.0 (3)	V2–C43	217.7 (2)
V1–C24	252.0 (3)	V2–C44	243.4 (2)

[a] Distance between the vanadium atom and the best plane of the η^8-cot ligand.

Figure 1 and an ORTEP drawing of the two molecules in Figure 2.

These drawings as well as the data in Table III show small differences between I and II. The most important feature of the molecular structure in the crystalline state is the bonding mode of the two cot ligands in the complex shown in Figure 2. One cot ligand is η^8-coordinated to the metal with a mean V–C distance of 229 ± 4 pm in I and 226 ± 4 pm in II,[15] whereas the second cot ring is bound in a 1,4-η^4 fashion.

The η^4-cot ligands in I and II are slightly twisted and the best planes of the coordinated parts (C21–C24 for I and C41–C44 for II) are bent away from coplanarity with the best planes of the corresponding η^8-cot ligands (C11–C18 for I and C31–C38 for II) of about 5.0 (2) and 7.7 (2)°, respectively. Such a deflection of an η^4-cot ligand is well documented for other η^4-cot complexes.[16] The V–C distances of the inner C atoms C22,23 and C42,43 in I and II, respectively, of the coordinated butadiene units are between 215 and 218 pm and hence considerably shorter than the corresponding V–C distances of the "terminal" C atoms C21,24 and C41,44, respectively, which are within the range 233–243 pm. An exception is the unusual bond length of 252.0 (3) pm between V1 and C24. The metal-bonded butadiene unit of the η^4-cot ligand shows no significant variation of the C–C bond lengths in both I and II while a significant C–C bond alternation is found only in the free butadiene part of II. The lack of a corresponding bond alternation in I can be explained by a more important thermal motion in the noncoordinated part of the η^4-cot ligand of I compared to II. An attentive comparison between I and II shows a slightly more tilted η^4-cot ligand in I than in II (compare the two projections in Figure 2).

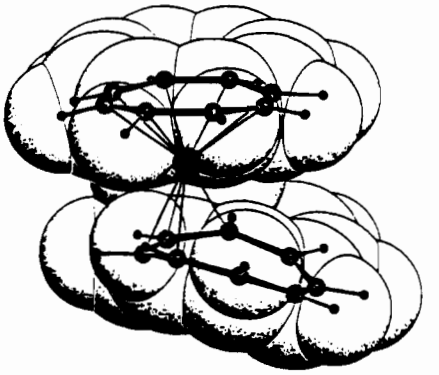

Figure 3. Space filling molecular model of **1** taking into account the van der Waals radii (SCHAKAL plot[21,22]).

The η^8-cot ligand is almost planar and the positions of the C atoms deviate in pairs from the best planes within +4 pm forming a very shallow boat conformation. This agrees well with the "short–short–long–long" alternation in the V–C distances, whereas no systematic short–long–short variation in the C–C distances can be found. From the ORTEP plots of I and II in Figure 2 it can be noticed that the C–H bonds in the (η^8-cot)V units are bent toward the V center. Although from X-ray structure analysis a considerable large uncertainty is normally inherent in the positional parameters of hydrogens, the distinct deviation of the C–H bond from the best plane of about 0–20° in the (η^8-cot)V unit[17a] confirms the results of EHMO calculations of Hoffmann and coworkers predicting a mean value of 10 + 6° in $M(CH)_n$ fragments.[17b]

Another noteworthy outcome of the X-ray structure analysis is the short distance between the best plane of the η^8-cot ligand and the vanadium atom of about 139 pm (see Table III). This is attributed to the large radius of the cot ring compared to other $(CH)_x$ ligands such as C_6H_6[18] and C_7H_7.[19] In order to have an equivalent overlap between the metal and the η^8-cot ligand similar to other vanadium complexes containing π-rings of smaller size, the metal center in **1** has to be immersed deeper inside the ligand sphere. As a consequence, the metal to ligand plane distance becomes considerably smaller than the van der Waals radius of the π-orbitals of $(CH)_x$ cycles, which are assumed to be on the order of 165–170 pm.[20] The resulting sterical shielding of the vanadium nucleus, illustrated in Figure 3, may contribute to the low reactivity for substitution reactions.

(15) The smaller V–C distances in II compared to I may be due to the larger thermal motion of the cot ring in II (compare ellipsoids in Figure 2, and note the 30% probability ellipsoids which fake smaller distances between atoms).

(16) E.g. $[Fe(cot)_2]$: Allegra, G.; Colombo, A.; Immirzi, A.; Bassi, I. W. *J. Am. Chem. Soc.* **1968**, *90*, 4455. $[Fe(\eta^4\text{-cot})(CO)_3]$: Dickens, B.; Lipscomb, W. N. *J. Chem. Phys.* **1962**, *37*, 2984. $[Zr(\eta^5\text{-}C_5Me_5)(1\text{–}4,\eta^4\text{-cot})(C_3H_5)]$: Highcock, W. J.; Mills, R. M.; Spencer, J. L.; Woodward, P. *J. Chem. Soc., Dalton Trans.* **1986**, 829. $[Nb(\eta^4\text{-cot})(\eta^5\text{-}C_9H_8Ph)(Me_2AsC_6H_4AsMe_2)]$: Schrock, R. R.; Guggenberger, L. J.; English, A. D. *J. Am. Chem. Soc.* **1976**, *98*, 903. $[Cr_2(cot)_3]$: Brauer, D. J.; Kruger, C. *Inorg. Chem.* **1976**, *15*, 2511.

(17) (a) Small values and negative signs of the distances (r) and angles (a) may be caused by a steric repulsion between the corresponding protons and those protons of the η^4-cot ligand which are positioned just in the opposite of the former protons and which are directed toward the η^8-cot ring. (b) Chen, M. M. L.; Elian, M.; Hoffmann, R.; Mingos, D. M. P. *Inorg. Chem.* **1976**, *15*, 1153.

(18) Duff, W.; Jonas, K. *J. Am. Chem. Soc.* **1983**, *105*, 5479.

(19) Engebretson, G.; Rundle, R. E. *J. Am. Chem. Soc.* **1963**, *85*, 5479.

(20) Allinger, N. L.; Miller, M. A.; Tyminski, I. J.; van Catledge, F. A. *J. Am. Chem. Soc.* **1968**, *90*, 1199.

(21) Johnson, C. K. ORTEP. A Fortran Thermal Ellipsoid Plot Program for Crystal Structure Illustration. Report ORNL-3794; Oak Ridge National Laboratory: Oak Ridge, TN, 1965.

(22) Keller, E. SCHAKAL-86-b (A FORTRAN Program for the Graphical Representation of Molecules and Crystallographic Models). Universität Freiburg, 1980.

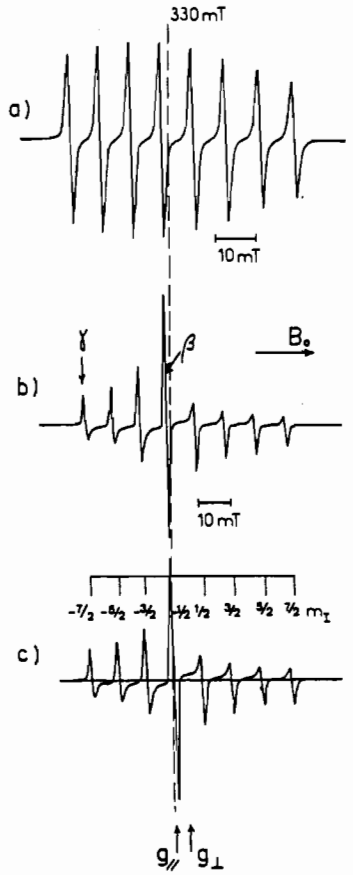

Figure 4. X-Band EPR spectra of $V(C_8H_8)_2$ in toluene solution: (a) spectrum of liquid solution at 298 K; (b) spectrum of frozen solution at 120 K; (c) spectrum simulated with parameters given in Table I.

Complex **1** is presently the second representative of V–cot complexes containing a (η^8-cot) ligand. The first example[23] is the mixed sandwich (η^8-cot)V[$(C_2H_5)C_2B_4H_4$] (**2**), the cot V unit of which is very similar to that in **1**.

The structure of **1** resembles the crude data of the X-ray structure analysis of the Ti analogue (η^8-cot)Ti(1-4,η^4-cot) (**3**), briefly published[24] in 1969, and is in accordance with the similarity of the IR-spectra[25] of **1** and **3**. NMR data for **3** showed a molecular fluxionality consisting of an interchange of hapticity between the two cot ligands.[10] No such NMR study is practical for looking into a potential fluctionality in **1** due to its low solubility and especially its paramagnetism.

Electron Paramagnetic Resonance

The EPR spectrum of **1** in toluene at room temperature is shown in Figure 4a. It exhibits the typical eight-line hyperfine pattern of a mononuclear vanadium complex with an unpaired electron interacting with the ^{51}V nucleus. This spectrum is identical with that reported by Hocks et al.,[5] and the g and vanadium hyperfine parameters are found to be

$$g_{av} = 1.985$$

$$^{V}A_{av} = \frac{1}{3}(^{V}A_{\parallel} + 2\,^{V}A_{\perp}) = -8.43 \text{ mT}$$

The signs of the hf parameters will be justified below. The spectrum obtained upon rapid cooling at 120 K is shown in Figure 4b. It is definitely different from that reported by Hocks et al.[5] but very similar to that of bis(benzene)vanadium,[12,26] $V(\eta^6\text{-}C_6H_6)_2$, and other vanadium sandwich compounds[27] (see also Table IV). The difference between our spectrum and the one previously reported[5] is due to the different solvents used, which are respectively toluene and benzene. The solubility of **1** is very low in benzene and the broad and intense line that was attributed to the perpendicular component of the spectrum is in fact due to a solid precipitate which gives a simple line undergoing exchange narrowing. The spectrum obtained after rapid cooling at 120 K in toluene, Figure 4b, is composed of an eight-line pattern corresponding to the perpendicular component of the **g** and ^{V}**A** tensors, with a strong fourth line resulting from the superposition of the parallel component with the $m_I = -1/2$ line of the perpendicular component. The parallel hyperfine (hf) pattern is not resolved because the parallel hf interaction $^{V}A_{\parallel}$ is smaller than the line width $\Delta B = 1.4$ mT. For this frozen-solution spectrum, simulation using the experimental parameters gave a very similar spectrum (Figure 4c).

Table IV. EPR Parameters of Vanadium Sandwich Compounds

	g_{av}[a]	$g_{\parallel}$[a]	$g_{\perp}$[a]	$^{V}A_{av}$, mT	$^{V}A_{\parallel}$,[b] mt	$^{V}A_{\perp}$, mT
1	1.985	2.001[c]	1.977[c]	−8.43 (2)	−2.01[c]	−11.64 (2)[c]
$V(bz)_2$[d]	1.986	2.002	1.979	−6.35 (5)	−0.65	−9.2 (5)
CpVCht[e]	1.987	2.005[f]	1.978	−7.41 (5)	−1.49[c]	−10.41 (5)

[a] ±0.001. [b] Calculated from $^{V}A = 3\,^{V}A_{av} - 2\,^{V}A_{\perp}$. [c] Obtained from calculated spectra. [d] g and $^{V}A_{\parallel}$ values obtained from powder samples of $V(bz)_2$ in $Cr(bz)_2$; see ref 26. [e] g and $^{V}A_{\parallel}$ values obtained from toluene solution; see ref 27. [f] Obtained from $g_{\parallel} = 3g_{av} - 2g_{\perp}$. [g] g and A values obtained from toluene solution.

The spin Hamiltonian parameters of **1** are reported in Table IV. The value $g_{\parallel} = 2.001$ of the **g** tensor is very close to the free-spin g value, which indicates that the singly occupied molecular orbital (SOMO) is essentially of metallic d_{z^2} character. Since this orbital is mainly nonbonding, we expect very weak interactions with π orbitals of the organic ligands and also very little perturbations from the axial **g** tensor, as it is effectively shown in the purely axial EPR spectrum of the frozen solution.

For an electron in a d_{z^2} orbital, the two components of the hyperfine tensor are given by the expressions[28]

$$^{V}A_{\parallel} = {}^{V}A_{iso} + \tfrac{4}{7}\alpha_1^2 P - \tfrac{1}{7}(g_{\perp} - g_e)P$$

$$^{V}A_{\perp} = {}^{V}A_{iso} - \tfrac{2}{7}\alpha_1^2 P + \tfrac{15}{14}(g_{\perp} - g_e)P \qquad (1)$$

where $^{V}A_{iso}$ is the isotropic interaction, the second term is the dipolar interaction, and the third term is the contribution of the spin–orbit coupling to the anisotropic hf interaction. In these expressions, the term P is given by

$$P = \frac{g\beta g_N \beta_N}{\langle r^3 \rangle} \qquad (2)$$

and α_1^2 is the coefficient of the d_{z^2} orbital in the SOMO. The spin–orbit coupling gives only a minor contribution to the anisotropic interaction, so that the amplitude of $^{V}A_{\parallel}$ and $^{V}A_{\perp}$ are mainly determined by $^{V}A_{iso}$ and the dipolar term. Since P is positive, the very small value of $^{V}A_{\parallel}$ implies $^{V}A_{iso} < 0$, and thus the signs of $^{V}A_{\parallel}$ and $^{V}A_{\perp}$ are both negative. The consequence of the spin–orbit coupling contribution is that the isotropic hf interaction $^{V}A_{iso}$ is slightly different from the hf parameter $^{V}A_{av}$ measured in liquid solution:

$$^{V}A_{iso} = {}^{V}A_{av} - \tfrac{2}{3}(g_{\perp} - g_e)P \qquad (3)$$

If we take a value of α_1 in the range 0.95–1, as expected for a nonbonding orbital, expressions 2 and 3 give P in the range P = +10.85 to +11.97 mT and $^{V}A_{iso} = -8.24 \pm 0.01$ mT.

Very slow cooling of the solution has a significant effect on the shape of the EPR spectrum. It causes toluene to crystallize instead of forming a gel, and in this case we often observed an increase of the $m_I = -1/2$ EPR line intensity while the other transitions are distorted and become less intense (Figure 5). In our opinion,

(23) Swisher, R. G.; Sinn, E.; Grimes, R. N. *Organometallics* **1984**, *3*, 599.
(24) Dietrich, H.; Soltwisch, M. *Angew. Chem.* **1969**, *81*, 785. *Angew. Chem., Int. Ed. Engl.* **1969**, *8*, 765.
(25) Hocks, L.; Goffart, J.; Duyckaersts, G.; Teyssie, P. *Spectrochim. Acta, A* **1974**, *30*, 907.
(26) Andrews, M. P.; Mattar, S. M.; Ozing, A. *J. Phys. Chem.* **1986**, *90*, 1037.
(27) Butcher, R. Ph.D. Thesis, Zurich, 1977; No. 5949.
(28) McGarvey, B. R. *J. Phys. Chem.* **1967**, *71*, 51.

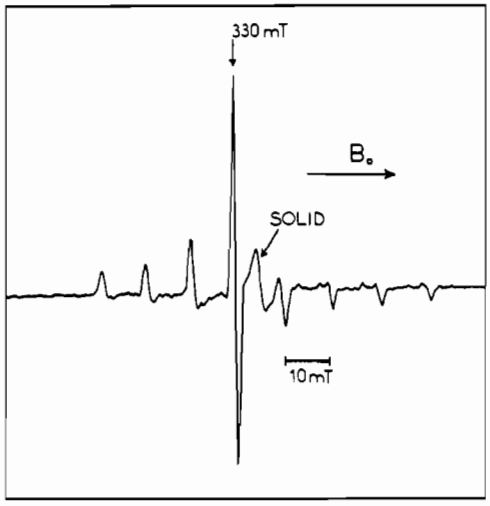

Figure 5. X-Band EPR spectrum of $V(C_8H_8)_2$ recorded at 120 K after very slow cooling.

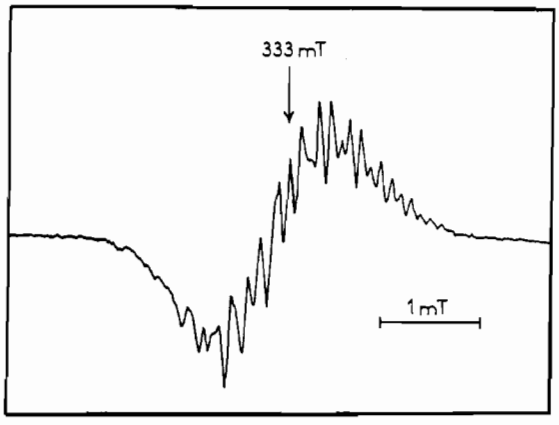

Figure 6. Proton hyperfine structure of the $m_I = -1/2$ EPR line of $V(C_8H_8)_2$ recorded at 120 K after very slow cooling. Conditions: microwave power 0.2 mW; modulation amplitude 0.04 mT.

this phenomenon is due to a partial orientation of the toluene crystallites along the magnetic field $\mathbf{B}_0$, which in turn results in a partial orientation of the molecules of the complex along $\mathbf{B}_0$ as shown by the increase in intensity of the $m_I = -1/2$ EPR lines, which is close to the parallel component of the spectrum. ENDOR experiments confirm this interpretation as will be shown below. The other effect of slow cooling is to oversaturate the solution, giving rise to the precipitation of solid **1** which appears as a broad single line growing between the $m_I = -1/2$ and $m_I = +1/2$ EPR transitions. The spectrum reported previously[5] is the extreme case where the EPR line of solid $V(C_8H_8)_2$ is largely predominant. This precipitation leaves a dilute solution, where line broadening which originates from dipolar interactions between isolated complexes is reduced and the hf interactions with the protons of the η^8- and the η^4-C_8H_8 rings become detectable. Figure 6 shows the proton hf structure of the $m_I = -1/2$ EPR transition after very slow cooling at 120 K. The microwave power and the modulation amplitude were set at low values (0.2 mW and 0.04 mT, respectively) in order to minimize the line broadening induced by saturation and overmodulation. This hf structure is not resolved below about 60–70 K, and the resolution enhancement upon increase of temperature is readily explained by the rapid motion of the C_8H_8 rings, which averages the dipolar part of the proton hf interactions. Nevertheless, the resolution remains too low to enable us to derive more information about intramolecular motion. More precise information concerning ring dynamics was obtained from ENDOR measurements.

Electron Nuclear Double Resonance

In a conventional powder or frozen solution ENDOR experiment, the magnetic field $\mathbf{B}_0$ is set at a given value within the EPR absorption envelope, and the intensity change of the EPR absorption is monitored upon radiofrequency field scan.[29] In that case the ENDOR response concerns only the subset of molecules which contribute to the EPR intensity at the chosen magnetic field setting, which is also called the observing field. If we saturate the so-called EPR turning points which correspond to particular molecular orientations, we can thus perform ENDOR with selection of molecular orientations.[30,31] For the frozen-solution EPR spectra depicted in Figures 4 and 5, we chose two magnetic field settings marked by arrows in Figure 4b. The first setting is the perpendicular $m_I = -7/2$ transition (field setting γ), which allows one to select complexes with a molecular axis (the z axis) perpendicular to the magnetic field $\mathbf{B}_0$. In that case $\mathbf{B}_0$ has an arbitrary orientation in the molecular xy plane because the **g** and vanadium hyperfine tensors are axial, and thus a setting of the magnetic field at this turning point gives a superposition of the ENDOR spectra arising from all the $\mathbf{B}_0$ orientations in the complex xy plane. The resulting spectrum is called a *two-dimensional* ENDOR spectrum. The other magnetic field setting of interest is the strong fourth line (field setting β), which contains both the parallel turning points and the perpendicular $m_I = -1/2$ turning point. At this field value we do not select any special molecular orientation since $\mathbf{B}_0$ assumes all the angles with respect to the xyz molecular frame. We obtain in that case a *powder* ENDOR spectrum. In order to facilitate the interpretation of this spectrum, we have taken advantage of the partial molecular orientation in the magnetic field upon slow cooling of the solution, as described above. The more complete this molecular orientation is, the stronger are the parallel components of the powder ENDOR spectra, which allowed us to attribute unambiguously the different ENDOR lines.

The major difficulty in the interpretation of the frozen solution ENDOR of **1** arose from the existence of two different types of vanadium to (η-C_8H_8) ring bonding which gave rise to three different kinds of hydrogens, namely (η^8-C_8H_8) and (1,4-η^4-C_8H_8) hydrogens of the carbon atoms directly bonded to the metal and the four terminal hydrogens of the η^4-C_8H_8 ring. These different

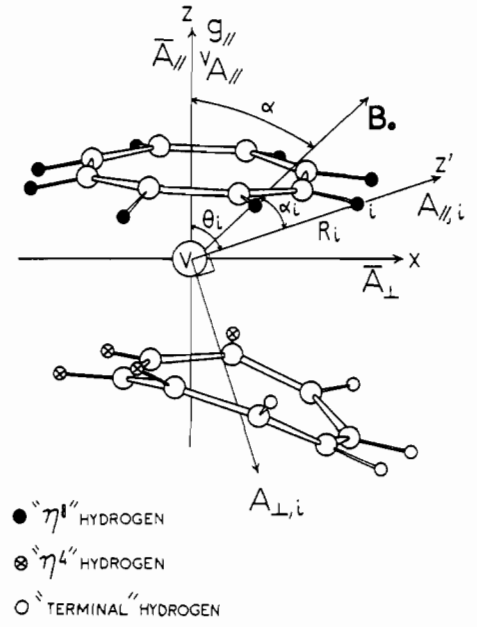

Figure 7. Schematic diagram representing the three types of protons and the relations between the molecular frame, the principal axes of the **g** and hyperfine tensors, and the magnetic field $\mathbf{B}_0$.

(29) (a) Rist, G.; Hyde, J. *J. Chem. Phys.* **1968**, *49*, 2449. (b) Rist, G.; Hyde, J. *J. Chem. Phys.* **1969**, *50*, 4532.
(30) Rist, G.; Hyde, J. *J. Chem. Phys.* **1970**, *52*, 4633.
(31) (a) Hurst, G. C.; Henderson, T. A.; Kreilick, R. W. *J. Am. Chem. Soc.* **1985**, *107*, 7294. (b) Attanasio, D. *J. Chem. Soc., Faraday Trans.* **1989**, *85*, 3927. (c) Yordanov, N. D.; Zdravkova, M.; Shopov, D. *Chem. Phys. Lett.* **1986**, *124*, 191. (d) Hoffman, B. M.; Martinsen, J.; Venters, R. A. *J. Magn. Reson.* **1984**, *59*, 110.

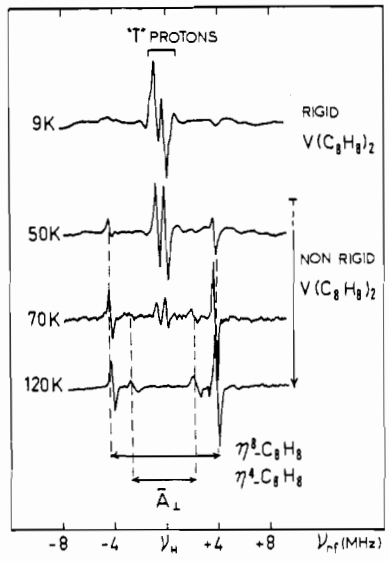

Figure 8. Temperature dependence of the *two-dimensional* ENDOR spectra of $V(C_8H_8)_2$ in frozen deuteriotoluene solution. Magnetic field setting γ was used (Figure 4b). Proton frequency: ν_H = 12.93 MHz. Modulation depth: 150 kHz. Microwave power: 8 mW at 9 K; 40 mW at 50, 70, and 120 K. Microwave frequency: 9516 MHz at 9–70 K; 9550.4 MHz at 120 K.

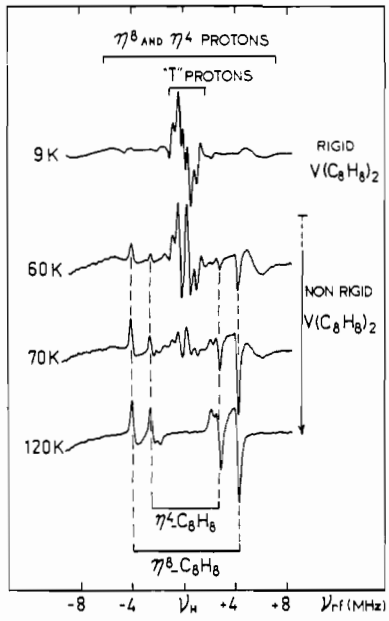

Figure 9. Temperature dependence of the *powder* ENDOR spectra of $V(C_8H_8)_2$ in frozen deuteriotoluene solution. Magnetic field setting β was used (Figure 4b). Proton frequency: ν_H = 14.34 MHz. Modulation depth: 150 kHz. Microwave power: 8 mW at 9 K; 40 mW at 60 K; 63 mW at 70 and 120 K. Microwave frequency: 9516 MHz at 9–70 K; 9550 MHz at 120 K.

protons will be hereafter designated as η^8, η^4, and T protons respectively. Figure 7 shows the orientations of the different **g** and hyperfine tensor axes with respect to the molecular framework. Under static conditions, i.e. without molecular motion, the z' axes of the proton hf tensors are nearly along the vanadium–proton directions. We may thus define at least four different families of angles θ between these axes and the molecular axis, which is also the z direction of the **g** and ^{51}V hf tensors. The variety of different protons results in a complicated and poorly resolved ENDOR spectrum, whatever the field setting chosen. A dramatic simplification is observed when intramolecular motions are in the fast exchange regime. In that case, the directions of the hf tensors become nearly parallel to the molecular axis and consequently the ENDOR line shape will depend more significantly on the field setting. Since the dipolar part of the hf interaction is partially averaged by the intramolecular motion, the distribution of ENDOR frequencies for each kind of protons is much narrower than in the slow-motion regime.

a. Results. Figure 8 shows some selected two-dimensional spectra recorded in rapid cooling conditions (field setting γ in Figure 4b) at 9, 50, 70, and 120 K. At 9 K, we observe essentially two strong ENDOR lines at frequencies close to the proton frequency ν_H. There is also some evidence of an unresolved structure which appears as shoulders flanking the two lines. The line shape resembles that generally observed for protons of solvent molecules[7] (also called matrix ENDOR[32]) which interacts with the unpaired electron spin only via purely point dipole–dipole interactions. In this work we used deuteriotoluene in order to avoid obtaining these matrix ENDOR lines. This allows one to attribute the matrix-like ENDOR lines of Figure 8 to the T protons of the (η^4-C_8H_8) ring, which are expected to give a purely dipolar hf interaction with the electron spin because of their remoteness. The broad and badly resolved lines on both sides of the central line are due to the closer η^8 and η^4 protons, which exhibit hf interactions with both Fermi contact and dipolar contributions. At this low temperature, all the intramolecular motions are very slow, and all the protons are thus chemically and magnetically nonequivalent because of the low molecular symmetry (point group C_s). This explains the lack of pronounced turning points for ENDOR of η^8 and η^4 protons.

At 30 K, a pair of narrow and dissymmetrical lines separated by 8.40 MHz start to grow and become more intense at 50 K. They belong to η^8 protons and are easily distinguished because the dipolar part of the hf interaction is now partially averaged by the rapid site exchange of protons due to the rapid rotation of the (η^8-C_8H_8) ring.[7] It should be noticed that the two lines are still dissymmetrical, which shows that we are not dealing with a purely single-crystal-like ENDOR spectrum.[30,31] This indicates that the principal axis of the motionally averaged hf tensor is not rigorously parallel to the molecular axis, which results from the low molecular symmetry produced by the motionless (η^4-C_8H_8) ring.

Three new modifications are observed between 50 and 70 K. First, the 8.40-MHz pair of lines becomes single crystal like, which implies that the proton hf tensor axis and the molecular axis are now strictly parallel. In addition, the central lines vanish while a pair of relatively broad and symmetrical lines separated by 5.44 MHz progressively grows in. These phenomena are more pronounced at higher temperature, and at 100 K the central lines are not longer apparent. All these new features are due to the onset of rapid rearrangement of the (η^4-C_8H_8) ring. This intramolecular motion, which reflects a rapid exchange of η^4 and T proton sites, explains the simultaneous disappearance of the central line and the appearance of the symmetrical 5.44-MHz pair of lines. The rapid motion of both rings produces a significant symmetrization of the complex, which could explain why all the ENDOR lines are now almost single crystal like.

The same features are also observed in the powder ENDOR obtained for the $m_I = -1/2$ EPR line (field setting β in Figure 4b), although the spectra are more complicated in that case, as shown in Figure 9. At 9 K, the T protons exhibit a powder-shape ENDOR spectrum with at least two pairs of lines. The broad and weak lines on each side of the strong central lines are due to turning points in the ENDOR of η^8 and η^4 protons. At 60 K, one observes the growth of relatively narrow lines of η^8 and η^4 protons in rapid motion regime. The central lines and the broad lines belonging to static T, η^8, and η^4 protons are still present, but they progressively decrease with increasing temperature and they completely vanish at about 100 K. Even at this temperature, ENDOR lines exhibit a pronounced powder shape, showing that the dipolar interactions are not completely averaged to zero by the rapid intramolecular motion of (η^8-C_8H_8) and (η^4-C_8H_8) rings.

b. ENDOR Parameters. Each i proton (i = 1–16) of complex **1** can be characterized by three parameters: the metal–proton distance R_i, the angle θ_i between the molecular axis z and the vanadium–proton interconnection line z', and the electron spin

(32) Hyde, J.; Rist, G.; Erikssion, L. E. G. *J. Phys. Chem.* **1968**, *72*, 4269.

density ρ_{Hi} at this proton. The vanadium–proton hf interaction A_i (α_i) is the sum of an isotropic part

$$A_{iso,i} = (8\pi/3)g\beta g_N\beta_N|\Psi_0(s)|^2\rho_{Hi} \quad (4)$$

where $|\Psi_0(s)|^2$ is the spin density at the hydrogen nucleus, and a dipolar part $A_{dip,i} = g\beta g_N\beta_N R_i^{-3}$:

$$A_i(\alpha_i) = A_{iso,i} + A_{dip,i}(3\cos^2\alpha_i - 1) \quad (5)$$

Here α_i is the angle between the magnetic field $\mathbf{B}_0$ and the vanadium proton axis. Expression 5 can be applied for **1** since the vanadium–proton distances are larger than 200 pm. The resulting hf tensor is nearly axial with components $A_{\parallel,i}$ and $A_{\perp,i}$ and with the tensor z' axis at an angle θ_i from the molecular axis. If we neglect the anisotropy of the **g** tensor, the ENDOR frequencies for the ith proton are given by the following expression for an arbitrary angle α_i:

$$\nu_i(m_s) = [(m_sA_{\parallel,i} - \nu_H)^2\cos^2\alpha_i + (m_sA_{\perp,i} - \nu_H)^2\sin^2\alpha_i]^{1/2} \quad (6)$$

If we choose the field setting γ on the EPR spectrum, we select molecules with $\mathbf{B}_0$ perpendicular to the molecular axis. In that case, the angle α_i can be assumed all the values in the range $\pi/2$ to $\pi/2 - \theta_i$. We thus expect a two-dimensional ENDOR spectrum for each proton i with two turning points for each transition at frequencies

$$\nu_i(m_s) = |m_sA_{\perp,i} - \nu_H|$$

$$\nu_i(m_s) = [(m_sA_{\parallel,i} - \nu_H)^2\sin^2\theta_i + (m_sA_{\perp,i} - \nu_H)^2\cos^2\theta_i]^{1/2} \quad (7)$$

In the case of the field setting β, there is no selection of molecular orientation and the angle α_i can take all the possible values. The resulting ENDOR spectrum has a powder shape with two turning points for each m_s transition given by

$$\nu_i(m_s) = |m_sA_{\parallel,i} - \nu_H|$$

$$\nu_i(m_s) = |m_sA_{\perp,i} - \nu_H| \quad (8)$$

In principle we may thus expect to measure $A_{\parallel,i}$, $A_{\perp,i}$, and θ_i for each proton by comparison of the two-dimensional and powder ENDOR spectra. As noted before, the crystal structure showed that the 16 hydrogen atoms can be classified into three types labeled η^8, η^4, and T. However, strictly speaking, all the vanadium–proton distances R_i, and hence the spin densities ρ_{Hi}, are different. This is true even for the η^8 protons, since V–C distances alternate in a "short–short–long–long" manner. We thus expect a distribution of the hf parameters $A_{\parallel,i}$ and $A_{\perp,i}$, resulting in a broad distribution of the ENDOR frequencies for the different turning points in the two-dimensional and powder ENDOR spectra. This most probably explains the very low resolution of the ENDOR at 9 K (Figures 8 and 9) so that we could not measure the hf parameters at this temperature where all the intramolecular motions are frozen.

Consequently, we focused our attention only on the ENDOR spectra obtained at higher temperatures. The motional narrowing results in a loss of information, which is however largely compensated by a good precision for the ENDOR frequencies. Since the distances R_i can be independently obtained from the X-ray structure, we used the motionally narrowed ENDOR spectra to obtain information about the spin densities ρ_{Hi} at protons and the characteristics of the molecular motions. Let us first consider the rapid rotation of the (η^8-C_8H_8) ring. Since this motion manifests itself as a rapid exchange of the eight proton sites, the isotropic and dipolar hf interactions $A_{iso,i}$ and $A_{dip,i}$ are averaged, leading to only two parameters

$$\bar{A}_{iso} = \tfrac{1}{8}\sum_{i=1}^{8}A_{iso,i} \qquad \bar{A}_{dip} = \tfrac{1}{8}\sum_{i=1}^{8}A_{dip,i}$$

In addition, the z axis of the averaged hf tensor is now parallel to the molecular axis (Figure 7) since the latter passes through the center of gravity of the ring, and the ENDOR frequencies are now given by

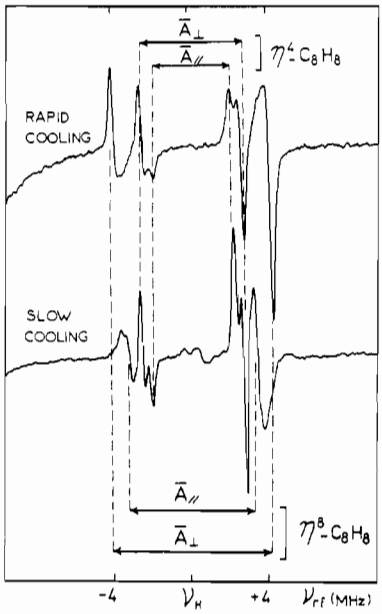

Figure 10. *Powder* ENDOR spectrum (field setting β) of $V(C_8H_8)_2$ at 100 K recorded under rapid- and slow-cooling conditions. Upon slow-cooling conditions, the partial alignment of the molecular axes along the magnetic field $\mathbf{B}_0$ produces an increase of the parallel turning points of the ENDOR lines, at the expense of the perpendicular turning points. Proton frequency: ν_H = 14.34 MHz. Modulation depth: 150 kHz. Microwave power: 40 mW.

$$\bar{\nu}(m_s) = [(m_s\bar{A}_\parallel - \nu_H)^2\cos^2\alpha + (m_s\bar{A}_\perp - \nu_H)^2\sin^2\alpha]^{1/2} \quad (9)$$

where α is the angle between $\mathbf{B}_0$ and the molecular axis. The two components $\bar{A}_\parallel$ and $\bar{A}_\perp$ of the motionally averaged hf tensor are related to $\bar{A}_{iso}$ and $\bar{A}_{dip}$ by

$$\bar{A}_\parallel = \bar{A}_{iso} + \bar{A}_{dip}(3\cos^2\bar{\theta} - 1)$$

$$\bar{A}_\perp = \bar{A}_{iso} - (\bar{A}_{dip}/2)(3\cos^2\bar{\theta} - 1) \quad (10)$$

where $\bar{\theta}$ is the mean angle of the eight vanadium–proton axes with the molecular axis. It follows that the isotropic interaction $\bar{A}_{iso}$ can be expressed by the relation

$$\bar{A}_{iso} = \tfrac{1}{3}(\bar{A}_\parallel + 2\bar{A}_\perp) \quad (11)$$

The parameters $\bar{A}_\parallel$ and $\bar{A}_\perp$ may be accurately measured from the ENDOR spectra by using the selection of molecular orientations.

Since the field setting γ allows one to select complexes with the molecular z axis perpendicular to $\mathbf{B}_0$, this corresponds to only one angle $\alpha = \pi/2$ in expression 9, which results in single-crystal-like ENDOR lines, and the ENDOR frequencies are now given by

$$\bar{\nu}(m_s) = |m_s\bar{A}_\perp - \nu_H| \quad (12)$$

Concerning the rapid rearrangement of the (η^4-C_8H_8) ring, the center of gravity of which is shifted from the molecular axis, we expect that the z' axis of the motionally averaged proton hf tensor is not rigorously parallel to the molecular axis z. In that case we expect to see ENDOR lines which are not purely single crystal like. However, examination of Figure 8 (spectrum at 120 K) shows that the ENDOR lines of η^4 protons are nearly symmetrical, so that we can use expressions 9 and 12 in a first approximation. The spectra at 120 K shown in Figure 8 give $\bar{A}_\perp(\eta^8)$ = +8.4 (0) MHz and $\bar{A}_\perp(\eta^4)$ = +5.4 (4) MHz for the η^8 and η^4 protons respectively. The parallel components $\bar{A}_\parallel(\eta^8)$ and $\bar{A}_\parallel(\eta^4)$ may be obtained from the powder ENDOR spectra recorded with the field setting β. Figure 10 shows two ENDOR spectra recorded at 100 K after rapid and very slow cooling. After rapid cooling, all the molecular orientations are equally probable and each m_s subset

of ENDOR lines should exhibit a powder shape with a strong perpendicular turning point at a frequency given by expression 12 and a weaker parallel turning point corresponding to $\alpha = 0$ in expression 9, which occurs at a frequency

$$\bar{\nu}(m_s) = |m_s\bar{A}_\parallel - \nu_H| \quad (13)$$

From the parallel turning points of η^4 protons ENDOR, we measure $\bar{A}_\parallel(\eta^4) = +3.8$ (4) MHz. The parallel turning points of η^8 proton ENDOR are not detectable because they are hidden by the perpendicular turning points of the η^4 protons. However, they are clearly observed when the complexes are partially oriented along $\mathbf{B}_0$ after slow cooling (Figure 10). In that case one observes a strong decrease of the perpendicular lines of η^8 protons and the appearance of two lines separated by $\bar{A}_\parallel(\eta^8) = +6.3$ (9) MHz. The same behavior is observed for the η^4 protons, with a significant increase of the parallel turning points.

If we return to the (η^8-C_8H_8) ring, the experimental values of $\bar{A}_\parallel(\eta^8)$ and $\bar{A}_\perp(\eta^8)$ give, with expression 10, $\bar{A}_{dip}(3\cos^2\bar{\theta} - 1) = -1.3$ (4) MHz. The crystal structure gives a mean V–C distance of 227 pm. If we take a C–H bond length of 108 pm and a deflection of the C–H bond from the C_8 plane of about 10°, we can estimate the theoretical anisotropic hf coupling at about $\bar{A}_{dip}(3\cos^2\bar{\theta} - 1) = -1.40 \pm 0.05$ MHz, which reasonably agrees with the experimental value.

The averaged isotropic interaction for the (η^8-C_8H_8) ring is equal to $\bar{A}_{iso}(\eta^8) = +7.7$ (3) MHz. If we neglect the small V–C bond alternation observed in the crystal structure, this value gives a good estimate of $A_{iso,i}(\eta^8)$, the isotropic interaction for each η^8 proton. The spin density $\rho_{Hi}(\eta^8)$ at each proton of the C_8H_8 ring is thus $\rho_{Hi}(\eta^8) = +5.4 \times 10^{-3}$.

As for the (η^4-C_8H_8) ring, the averaged hf tensor gives $\bar{A}_{iso} = +4.9$ (1) MHz. The motion of the ring results in a rapid exchange of proton sites of the coordinated butadiene unit (1–4,η^4 protons) and of the terminal protons of the noncoordinated butadiene unit. Since these two kinds of protons are characterized by isotropic coupling constants $A_{iso,i}(\eta^4) > 0$ with $i = 1$–4 for η^4 protons and $A_{iso,i}(T) \approx 0$ with $i = 5$–8 for terminal protons, the isotropic interaction for the static η^4 protons may be estimated from $A_{iso,i}(\eta^4) \approx 2\bar{A}_{iso}(\eta^4) \approx +9.8$ MHz, which corresponds to a spin density $\rho_{Hi}(\eta^4) = +6.9 \times 10^{-3}$. This value is larger than that measured for the η^8 protons, which corresponds to the fact that the V–C distances (215–218 pm) are shorter for the coordinated butadiene unit than for the (η^8-C_8H_8) unit (226–229 pm). The two parameters $\bar{A}_{iso}(\eta^4)$ and $\bar{A}_{iso}(\eta^8)$ are responsible for the proton hf structure of the EPR lines of **1** in frozen solution (Figure 6).

Molecular Motion in Frozen Solution

ENDOR spectroscopy provides insight into molecular dynamics, which strongly affect the ENDOR line shape as shown above by the temperature dependence of the spectra in the temperature range 9–130 K (Figures 8 and 9). In frozen solutions of **1**, all the spectral modifications up to 130 K are due to fast rearrangement of η^8- and η^4-bonded (C_8H_8) rings. This intramolecular motion manifests itself as a rapid exchange of sites of protons experiencing different interactions with the unpaired electron spin.

If we consider the simple case of a hydrogen jump between two positions A and B, the modification of the corresponding ENDOR spectrum will depend on the jump rate k relative to the characteristic frequency $\delta\nu = |\nu_A - \nu_B|$ of the ENDOR experiment, where ν_A and ν_B are one m_s set of ENDOR frequencies of the proton in the two positions. In the slow-exchange regime, i.e. for $k \ll 2\pi\delta\nu$, there are two independent ENDOR lines at frequencies ν_A and ν_B with line width $\Delta\nu$ on the order of $\Delta\nu = \Delta\nu_0 + 1/\pi\tau$, where $\tau = 1/k$ and where $\Delta\nu_0$ is the line width in the limiting case $k = 0$. In the fast-exchange regime, i.e. for $k \gg 2\pi\delta\nu$, the two ENDOR lines coalesce to give a single line at a frequency $\bar{\nu} = (\nu_A + \nu_B)/2$. The intermediate regime is that where the two lines strongly broaden and coalesce. The powder ENDOR spectrum at 9 K shown in Figure 9 corresponds to the situation where $k \ll 2\pi\delta\nu$ for all the intramolecular motions. In the case of η^8 protons, which individually bear about the same electron spin densities and which differ only by their dipolar interactions for a given orientation of the magnetic field, the characteristic frequency $\delta\nu$ may be estimated as

$$\delta\nu = \tfrac{1}{2}[A_{\parallel,i}(\eta^8) - A_{\perp,i}(\eta^8)] \approx \tfrac{3}{2}A_{dip,i}(\eta^8) \approx 4.5 \text{ MHz}$$

In the case of the (η^4-C_8H_8) intramolecular motion, which can be pictured as a migration of the metal–butadiene bonds around the ring, a terminal proton characterized by a zero electron spin density, $\rho_{Hi} \approx 0$, experiences a jump to a position where the spin density is relatively high, i.e. $\rho_{Hi}(\eta^4) \approx +6.9 \times 10^{-3}$. The characteristic frequency is thus dominated by the isotropic interaction and may be estimated to be $\delta\nu \approx \bar{A}_{iso}(\eta^4) \approx 5$ MHz. We have already noted that the rotation of the η^8-C_8H_8 ring reaches the fast exchange regime at a lower temperature (about 30 K) than the metal–carbon bond migration within the η^4-C_8H_8 ring, for which this regime is clearly observable at about 60 K. Since the characteristic frequencies for these two kinds of motions are very similar, this difference in temperature could be attributed to lower activation energies for the η^8-C_8H_8 rotation.

If each kind of intramolecular motion could be characterized by a single activation energy, we would expect a progressive modification of the ENDOR spectrum from the slow- to the fast-exchange regime upon increasing the temperature, as observed for $V(bz)_2$ diluted in a crystalline matrix.[11] In the case of [V-(C_8H_8)$_2$] in frozen solution, examination of Figures 8 and 9 shows that, between 50 and 70 K, ENDOR features of "static" η^8 and η^4 rings always coexist with the motionally narrowed lines of these rings. Increasing the temperature results only in decrease of intensity of the ENDOR features for the "static" rings. This indicates that both $k \ll 2\pi\delta\nu$ and $k \gg 2\pi\delta\nu$ regimes are present at a given temperature, which demonstrates that intramolecular motions have several activation energies. This behavior shows that η^8 and η^4 motions are governed by intermolecular rather than intramolecular potentials. The intermolecular potential should vary from site to site in the solid-state matrix, most probably because the geometry of the solvent cages in the frozen solution are not well-defined. Such control of ring motion by intermolecular potentials has already been demonstrated for [V(C_6H_6)$_2$] in single crystals[11] or polycrystalline matrices.[12] The existence of a distribution of activation energies seems to be a common feature for ring rotation in frozen solutions.[7,8,11]

It has already been demonstrated by NMR on diamagnetic η^4-C_8H_8 complexes[33] that the migration of the metal–carbon bond around the ring occurs via a [1,2] shift mechanism, which is characterized by a low activation energy. The other mechanisms, such as for example a [1,3] shift or random shifts, are forbidden and are thus characterized by higher activation energies. In the case of the allowed [1,2] shift mechanism, the motion simply results in migration of the butadiene unit around the ring, which preserves both slippage and bending of the η^4-C_8H_8 ring with respect to the (η^8-C_8H_8) one. The dissymmetry of the V–(1–4,η^4-C_8H_8) fragment is thus conserved, and we should expect motionally narrowed ENDOR lines that are not purely single crystal like. However there is experimental evidence that in the regime of fast intramolecular motion, **1** bears an apparent axial symmetry, giving single-crystal-like ENDOR lines as observed in more symmetrical complexes.[7,8] Thus the question arises whether another kind of rearrangement of the (η^4-C_8H_8) fragment could occur, as for example a rapid alternation of the bound butadiene unit (1–4,η^4 protons) and the free butadiene unit (T protons). In that case, we would expect the V–(η^4-C_8H_8) fragment to assume an intermediate configuration of the type (1,2,5,6-η^4-C_8H_8). A rapid motion of this type should give a complex of a higher apparent symmetry. This alternative would be in better agreement with our experimental results.

Another possible type of fluxionality is the rapid alternation of η^4- and η^8-bonded rings as already demonstrated by NMR studies of diamagnetic M(C_8H_8)$_2$ with M = Ti, Ta, and Nb.[9,10] In order to search for this intramolecular motion, we studied the evolution upon slow-cooling conditions of the high-frequency m_s

(33) Mann, B. E. *Adv. Organomet. Chem.* **1988**, *28*, 397.

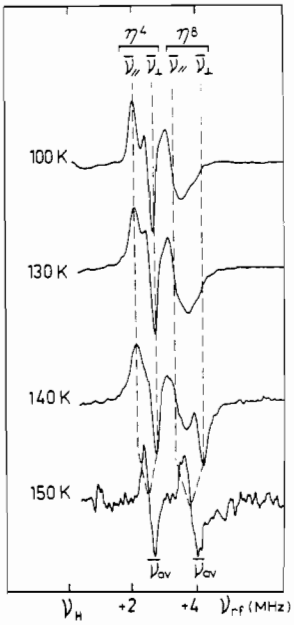

Figure 11. Effect of slow cooling on the $m_s = -1/2$ sets of ENDOR lines of $V(C_8H_8)_2$. Magnetic field setting β was used. Proton frequency: ν_H = 14.34 MHz. Modulation depth: 150 kHz. Throughout the temperature range 150–100 K, the η^8- and η^4-C_8H_8 rings are in the fast-motion regime. At 150 K, the complexes undergo rapid tumbling in solvent cages. At 140 K, the complexes are in the slow tumbling regime, without preferential orientations in solvent cages. At 130 K, the complexes are preferentially aligned along the magnetic field $\mathbf{B}_0$. Microwave power: 40 mW at 100 K; 126 mW at 130 K; 200 mW at 140 and 150 K. Microwave frequency: 9563 MHz.

set of ENDOR lines recorded with the field setting β ($m_I = -1/2$ EPR line). The results are reported in Figure 11. At temperatures above 160 K, the solution is liquid and we could not detect any ENDOR response, most probably because the maximum of rf power available (100 W) was too low in our ENDOR setup. At 150 K the EPR spectrum is that of the crystallized solution (Figure 5), and we observe two single crystal-like ENDOR lines at frequencies $\nu_H + {}^1/_2\bar{A}_{iso}(\eta^4)$ and $\nu_H + {}^1/_2\bar{A}_{iso}(\eta^8)$, which indicates that the η^4–η^8 alternation does not occur or is only in the slow-motion regime. In the fast regime, we should expect a single line at a frequency

$$\nu_H + {}^1/_4[\bar{A}_{iso}(\eta^4) + \bar{A}_{iso}(\eta^8)]$$

The characteristic frequency of the ring alternation being $\delta\nu = {}^1/_2[\bar{A}_{iso}(\eta^8) - \bar{A}_{iso}(\eta^4)]$, we may only give an upper limit $k \ll 9 \times 10^6\ s^{-1}$ at 150 K for this kind of intramolecular motion. Its observation needs an ENDOR investigation at higher temperatures in liquid solution, which could not be performed in our study.

Although the ring alternation is very slow at 150 K, it should be noted that the ENDOR lines are single crystal like, in spite of the fact that, at the field setting β, one cannot select any molecular orientation. We already noted that the ring rearrangements result only in a partial averaging of the dipolar hf interactions. The single-crystal-like ENDOR lines at 150 K show that the remaining anisotropy is now completely averaged out to zero. This shows the presence of a fast tumbling motion of **1** in cages of the toluene crystallites. In that case we expect a complete averaging of the dipolar interactions, without any effect on the isotropic ones. The tumbling rate is larger than the remaining proton hf anisotropy, (i.e. $k \gg \pi|\bar{A}_\perp - \bar{A}_\parallel| \approx 6 \times 10^6\ s^{-1}$), but smaller (i.e. $k \ll 10^9\ s^{-1}$) than the anisotropy of the ^{51}V hf tensors. At temperatures below 150 K, the molecular tumbling in solvent cages reaches the slow-exchange regime. At 140 K, the single-crystal-like shapes of the two ENDOR lines become powder shaped with the rise of perpendicular and parallel turning points at frequencies $\bar{\nu}_\parallel$ and $\bar{\nu}_\perp$ for both rings (Figure 11). However, the orientation of the molecules in the solvent cages is not achieved at this temperature, as demonstrated by the strong perpendicular turning point of the (η^8-C_8H_8) protons. This turning point almost disappears at 130 K, which indicates that a significant part of $[V(C_8H_8)_2]$ complexes are aligned along the magnetic field $\mathbf{B}_0$ at this temperature. ENDOR data are given in Table V.

Table V. ENDOR Parameters (MHz) of $[(\eta^4\text{-}C_8H_8)V(\eta^8\text{-}C_8H_8)]$ in Frozen Deuteriotoluene Solution

	$A_\parallel$	$A_\perp$	A_{iso}
η^8 protons[a]	+6.3 (9)	8.40	+7.7 (3)
η^4 protons[a]	+3.8 (4)	+5.44	+4.9 (1)

[a] Values corresponding to the regime of fast intramolecular motion. T = 120 K.

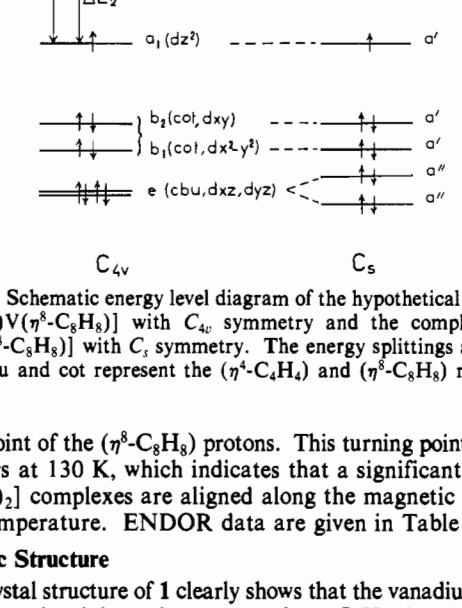

Figure 12. Schematic energy level diagram of the hypothetical complex $[(\eta^4\text{-}C_4H_4)V(\eta^8\text{-}C_8H_8)]$ with C_{4v} symmetry and the complex $[(\eta^4\text{-}C_8H_8)V(\eta^8\text{-}C_8H_8)]$ with C_s symmetry. The energy splittings are arbitrary. Cbu and cot represent the (η^4-C_4H_4) and (η^8-C_8H_8) rings, respectively.

Electronic Structure

The crystal structure of **1** clearly shows that the vanadium atom is bonded to the eight carbon atoms of one C_8H_8 ring (cot unit) and to four carbon atoms of the other C_8H_8 ring. Since the other four carbon atoms do not participate in the bonding, it is safe to assimilate the 1–4,η^4-bonded ring to a butadiene unit C_4H_6 (bu unit). Unfortunately the symmetry of the complex is very low (C_s symmetry), so that strictly speaking we cannot take advantage of the simple notation of high-symmetry groups. However, we can understand the bonding characteristics of **1** by considering successively the (V–cot) fragment with C_{8v} symmetry, the interactions between this fragment and a cyclobutadiene unit C_4H_4 (cbu unit), which reduces the symmetry to C_{4v}, and finally the lowering of the symmetry to C_s if we replace the cbu by a (1–4,η^4-C_8H_8) ring. In both cases the nature of the bonding remains the same, but the symmetry is different. The e_2 energy level of the cot ring being lower than that of the metal 3d levels, we may reasonably assign the formal charge (2–) in (cot^{2-}) to a 10-electron aromatic system.[34] Since the e level of cyclobutadiene has about the same energy as the e_2(cot) level,[35] we may also assign the formal charge (2–) in (cbu^{2-}) to a 6-electron aromatic system. We may thus formally represent this 17-electron system as [$cot^{2-}V^{4+}cbu^{2-}$], which has a d^1 configuration.

In C_{8v} symmetry, the metal 3d levels split into $a_1(d_{z^2})$, e_1 (d_{xz},d_{yz}), and e_2 ($d_{x^2-y^2}$,d_{xy}) levels. The vanadium–cot bonding takes place through electron donation from the filled e_2(cot) orbitals to the empty $e_2(d_{x^2-y^2},d_{xy})$ orbitals, the latter taking an antibonding character. The bonding of the (V–cot) fragment to a (cbu) unit has two effects. The first is to reduce the symmetry to C_{4v}, which splits the e_2 levels into b_1 and b_2 levels, the antibonding b_1* and b_2* having respectively $d_{x^2-y^2}$ and d_{xy} characters (Figure 12). The $a_1(d_{z^2})$ and $e(d_{xy},d_{yz})$ levels are not affected. The (V–cbu) bonding takes place through electron donation from the filled e(cbu) orbitals to the empty $e(d_{xz},d_{yz})$ metal orbitals,

(34) Clack, D. W.; Warren, K. D. *Inorg. Chim. Acta* **1977**, *24*, 35.
(35) Clack, D. W.; Warren, K. D. *Struct. Bonding*, **1980**, 39.

which thus take an antibonding character. At this stage, the bonding characteristics are very close to those of [CpTicot], if we exclude the splitting of the e_2 levels.[34] By comparison with this complex and using the fact that the e_1 (or e in C_{4v}) interactions increase as the ring size decreases,[35] we can propose the following sequence of energy levels:

$$e(cbu) < b_1(cot), b_2(cot) < a_1(d_{z^2}) < b_1^*(d_{x^2-y^2}), b_2^*(d_{xy}) < e^*(d_{xz},d_{yz})$$

The electronic configuration of [cbuVcot] is thus e^4,b_1^2,b_2^2,a_1, with an unpaired electron in the nonbonding $a_1(d_{z^2})$ orbital, yielding the $^2A_1$ ground state. Now, if we take into account the real structure of **1**, its symmetry is lowered to C_s, which results in two effects (Figure 12): (i) Each e level is split into two a'' levels with d_{xz}, d_{yz} characters. However, this splitting should have no significant effect on the metal–ligand interaction since the vanadium–(1–4,η^4-C_8H_8) bonding remains independent of the vanadium–(η^8-C_8H_8) bonding. (ii) The partially occupied, nonbonding $a'(d_{z^2})$ level (a_1 in C_{4v} symmetry) is now mixed with the bonding b_1,b_2 and antibonding b_1^*,b_2^* molecular orbitals with cot, $d_{x^2-y^2}$, and d_{xy} characters. It thus appears that the low symmetry of the (η^4-C_8H_8)V fragment essentially perturbs the (η^8-C_8H_8)V one.

Although we formally described the title compound as a [$bu^{2-}V^{4+}cot^{2-}$] complex, the net charge on the metal should lie between (4+) and 0, depending on the amount of ligand to metal electron donation. The hf parameter P given in expression 2 depends on the charge at the vanadium atom, and amounts to +18.4, +16.1, +13.8, +11.5, and +9.2 mT for V^{4+}, V^{3+}, V^{2+}, V^+, and V^0, respectively.[36] A linear interpolation shows that the experimental value of P for **1** corresponds to a net charge of about +0.7 to +1.2. These values are close to the charges +0.3, +0.4, and +1.0 found for [CpTicot] by MO calculations,[34] ESCA,[37] and EPR[38] measurements, respectively.

EPR also gives information on the structure of the SOMO. As noted above, the parallel g factor $g_\parallel = 2.001$ is very close to the free-spin value, which constitutes the "fingerprint" of a d_{z^2} ground state for which we expect $g_\parallel = g_e$. However, taking into account the low symmetry effects discussed above, the SOMO should contain contributions from metal $d_{x^2-y^2}$ and d_{xy} orbitals. However, such contributions should result in a deviation of $g_\parallel$ from the free-spin value, which is not observed experimentally. Another effect of the low symmetry of **1** should be the splitting of $g_\perp$ into two components g_x and g_y because of the splitting of the antibonding e* level. The lack of observable consequence of the low symmetry of **1** suggests that we may conserve the symmetry labels of the C_{4v} point group to describe the MO's.

Finally we have also strong evidence that the admixture of hydrogen s orbitals, carbon $2p_z$ orbitals and metal $d_{x^2-y^2}$ and d_{xy} orbitals in the SOMO are very small. The admixture α_2 of the metal 4s orbital is also very small, as demonstrated by the vanadium isotropic hf interaction $^V\!A_{iso} = 8.2$ mT. This admixture should introduce a positive contribution $\alpha_2^2\,{}^V\!A_{iso}(4s) = (+9.32\alpha_2^2)$ mT.[36] On the contrary, a spin density α_1^2 in the d_{z^2} orbital gives only a small negative contribution $\alpha_1^2\,{}^V\!A_{iso}(3d)$ due to spin polarization of inner s orbitals, and the resulting interaction $^V\!A_{iso} = -8.25$ mT is the sum of the two components. $^V\!A_{iso}(3d)$ is of the order of −7 mT for a V^{4+} ion,[39] but this value is too small to explain the isotropic coupling in **1** since it gives a negative sign for $\alpha_2^2\,{}^V\!A_{iso}(4s)$. It is known however that $A_{iso}(3d)$ increases as the charge at the metal decreases. For example, it increases[36] by 22% from Ti^{3+} to Ti^0. Assuming a charge of (1+) at vanadium, this should give $^V\!A_{iso}(3d) \approx -8.5$ mT for a pure d_{z^2} ground state orbital in **1**, which is very close to the experimental value. The limiting values for α_1 and α_2 are in that case $\alpha_1 > 0.98$ and $\alpha_2 < 0.05$, which strongly confirms that the SOMO is mainly d_{z^2}. In comparison, α_1 is equal to 0.96 in [CpVcht] (cht = η^7-C_7H_7)[40] and in [CpTicot].[34]

Conclusion

X-ray diffraction studies in conjunction with EPR and ENDOR on the title compound provided the following information:

The two cot rings exhibit different hapticities with regards to their bonding to vanadium and adapt their geometries to yield a 17-electron compound.

EPR parameters show that the singly occupied molecular orbital is primarily of nonbonding d_{z^2} character, and is not perturbed by the low symmetry induced by the (η^4-C_8H_8) ring.

Variable-temperature ENDOR spectroscopy revealed molecular fluxionality in the solid state at temperatures as low as 30 K. These are the rotation of the (η^8-C_8H_8) ring around the molecular axis and the fluxionality of the (η^4-C_8H_8) ring detectable at 50 K, both being controlled by intermolecular potentials. There was no evidence of any fast η^8–η^4 ring alternation in the frozen glassy or polycrystalline solution phases.

Finally, fast molecular tumbling of the complex occurs in polycrystalline solution just below the freezing point. This tumbling is slowed down at lower temperatures, and the complex partially orientates along the magnetic field in the solvent cages.

From these results it can be suggested that in the frozen or polycrystalline states, the solvent cages formed take a variety of sizes such that the intramolecular motions of the complex molecules confined in them have a whole range of activation energies. The cavity volume is however sufficiently large to allow these motions to occur at very low temperatures. In the polycrystalline phase the solvent crystallites are partially oriented along the magnetic field, and the cavities have probably an elongated form. This geometry constraint imposes the complex molecules to assume a preferential orientation inside the cage.

Acknowledgment. We are grateful to Mrs. J. Hénique and Mrs. D. Simons for technical assistance.

Supplementary Material Available: Listings of fractional atomic coordinates with standard deviations, least-squares planes, bond distances and angles, and experimental parameters of the X-ray structure analysis and crystal data (29 pages); a table of observed and calculated structure factors (32 pages). Ordering information is given on any current masthead page.

(36) Raynor, J. B.; Goodman, G. *Adv. Inorg. Chem. Radiochem.* **1970**, 13.
(37) Vliek, M.; Groenenboom, C. J.; de Lielfde Meijer; Jellinek, F. *J. Organomet. Chem.* **1975**, *97*, 67.
(38) Samuel, E.; Labauze, G.; Vivien, D. *J. Chem. Soc., Dalton Trans.* **1979**, 956.
(39) Coke, F. G.; Dix, A. N.; Green, J. L.; Perutz, R. N.; Seddon, E. A. *Organometallics* **1983**, *2*, 1150.
(40) Clack, D. W.; Warren, K. D. *Theor. Chim. Acta* **1977**, *46*, 313.